Hydrogenated amorphous silicon oxide containing a microcrystalline silicon phase and usage as an intermediate reflector in thin-film silicon solar cells

A. Lambertz, T. Grundler, and F. Finger

Additional information on J. Appl. Phys.

Hydrogenated amorphous silicon oxide containing a microcrystalline silicon phase and usage as an intermediate reflector in thin-film silicon solar cells

A. Lambertz,[a)] T. Grundler,[b)] and F. Finger
IEK5-Photovoltaik, Forschungszentrum Jülich, 52425 Jülich, Germany

To further improve the stability of amorphous/microcrystalline silicon (a-Si:H/μc-Si:H) tandem solar cells, it is important to reduce the thickness of the a-Si:H top cell. This can be achieved by introduction of an intermediate reflector between the a-Si:H top and the μc-Si:H bottom cell which reflects light back into the a-Si:H cell and thus, increases its photocurrent at possibly reduced thickness. Microcrystalline silicon oxide (μc-SiO$_x$:H) is used for this purpose and the trade-off between the material's optical, electrical and structural properties is studied in detail. The material is prepared with plasma enhanced chemical vapor deposition from gas mixtures of silane, carbon dioxide and hydrogen. Phosphorus doping is used to make the material highly conductive n-type. Intermediate reflectors with different optical and electrical properties are then built into tandem solar cells as part of the inner n/p-recombination junction. The quantum efficiency and the reflectance of these solar cells are evaluated to find optical gains and losses due to the intermediate reflector. Suitable intermediate reflectors result in a considerable increase in the top cell current density which allows a reduction of the a-Si:H top cell thickness of about 40% for a tandem cell while keeping the current density of the device constant. © *2011 American Institute of Physics*. [doi:10.1063/1.3592208]

I. INTRODUCTION

For thin-film silicon solar cells, a popular cell configuration is the amorphous/microcrystalline silicon (a-Si:H/μc-Si:H) tandem, which consists of a high bandgap a-Si:H top cell and a lower bandgap μc-Si:H bottom cell. To reduce the effect of light-induced degradation on the cell performance, the amorphous top cell's thickness has to be kept as low as possible, which thus delivers a low photo current.[1,2] To achieve high efficiencies, the currents generated by top and bottom cell have to be well balanced. In order to obtain a sufficient top cell photocurrent the amount of light absorbed in the top cell can be increased by using an intermediate reflector layer (IR). The effects of intermediate reflectors for such cell configurations have been evaluated in model studies.[3–5] The reflector has to fulfill the following requirements:

- reflect shorter wavelength light back into the top cell.
- be transparent for the longer wavelength light which is used by the bottom cell.
- conduct the current between the cells.
- serve as a nucleation layer for the subsequent layer in case those are microcrystalline.

Several materials have been already investigated for this purpose. Among them are transparent conductive oxides like zinc oxide (ZnO).[6–8] The material has a refractive index of around two and its bandgap is higher than 3 eV. With doping, ZnO can be made highly conductive which on the one hand is wanted to keep the series resistance of the device low, but on the other hand a too high planar conductivity might require an additional laser structuring step for interconnecting the cells into modules. Furthermore typical preparation processes like low pressure chemical vapor deposition (LPCVD) or magnetron sputtering and process temperatures might be incompatible with the tandem device preparation technology.

Other approaches start from dielectric materials like SiN and SiO$_x$ which can be prepared with a wide range of optical properties but often are difficult to be doped conductive enough.[9]

In the present study, we investigate phosphorous doped hydrogenated microcrystalline silicon oxide as intermediate reflector.

The material is a phase mixture of microcrystalline silicon (μc-Si:H) with amorphous silicon oxide (a-SiO$_x$:H) where the phosphorus doping mainly affects the μc-Si:H phases. The two phases can be thought of as if delivering the required optical and electrical properties individually: The oxygen rich amorphous phase supplies low-refractive index and high-optical transparency. The n-type microcrystalline silicon phase ensures sufficient electrical conductivity in direction of the current flow between the component cells while the lower electrical conductivity in planar direction is beneficial for the interconnection to a module. In spite of the obvious two-phase nature of the material[10] we will call it μc-SiO$_x$:H in the following for simplicity. A number of studies including successful application of silicon oxide based intermediate layers have been already reported.[11–17] Furthermore, the material is a potential candidate for the use as window layer due to its combination of sufficient conductivity and high bandgap.[18]

Here, we present a detailed description of the μc-SiO$_x$:H material development, with a focus on the relationship between the deposition parameters and the material properties.

a)Electronic mail: a.lambertz@fz-juelich.de. FAX: +49-(0)2461-613735.
b)Present address: E-I2, Helmholtz-Zentrum Berlin, Hahn-Meitner-Platz 1, 14109 Berlin.

TABLE I. Overview of the flow rates for the SiO_x films and the corresponding symbols used in the figures.

hydrogen dilution $\phi_{SiH_4}:\phi_{H_2}$	Symbol	SiH_4-flow	CO_2-flow	H_2-flow	PH_3-flow
[sccm]: [sccm]		[sccm]	[sccm]	[sccm]	[sccm]
1:100	□	0.98	0–7	100	0.02
1:200	○	0.98	0–7	200	0.02
2:500	◇	1.96	0–14	500	0.04
1:500	☆	0.98	0–7	500	0.02
1:1000	+	0.98	0–7	1000	0.02

Guidelines for selection of material with desired properties as intermediate reflector are described and the successful application in thin-film silicon solar cells is demonstrated with a possible top cell thickness reduction by 40% while maintaining the total tandem cell current.

II. EXPERIMENT

A. Microcrystalline silicon oxide preparation

Silicon oxide layers were deposited in a plasma enhanced chemical vapor deposition (PECVD) multi chamber system using an excitation frequency of 13.56 MHz at a substrate temperature of 185 °C. The substrates were 100 cm^2 glass substrates type Corning Eagle 2000. The deposition pressure was 4 mbar and the power density 0.35 W/cm^2 with respect to the electrode area. The process gases used were silane (SiH_4) with an addition of 2% phosphine (PH_3) as dopant source, carbon dioxide (CO_2) and hydrogen (H_2). For simplicity we will refer to the PH_3/SiH_4 mixture as "SiH_4" in the following when describing the gas flow compositions, ignoring therefore the small (2%) amount of PH_3 and keeping in mind that the dopant gas concentration with respect to the silane gas will be always 2%, while the concentration with respect to the $[SiH_4 + CO_2]$ gas flow will vary depending on the respective CO_2 gas flow.

The material process optimization was mainly performed as a function of the CO_2 gas flow for a given hydrogen dilution, considering the CO_2 gas flow the main parameter which will determine the desired optical properties while both the CO_2 flow as well as the hydrogen dilution will strongly affect the crystallinity of the material or better to say the transition between highly crystalline and amorphous/microcrystalline mixed-phase material.

Frequently, we will use the ratio between the CO_2-flow ϕ_{CO_2} and the SiH_4-flow ϕ_{SiH_4}

$$r_{CO_2} = \frac{\phi_{CO_2}}{\phi_{SiH_4}} \qquad (1)$$

for presentation of the data

Also of great importance is the hydrogen dilution (H_2 dil.) which will be given in the form

$$H_2 dil. = \phi_{SiH_4} : \phi_{H_2} \qquad (2)$$

with each flow, Φ_{H_2} and Φ_{SiH_4} measured in sccm, i.e., H_2 dil. = 2:500 stands for a SiH_4-flow of 2 sccm and a H_2-flow of 500 sccm. Important to note is that the hydrogen dilu-

tion is related to the SiH_4 only and not to the sum of SiH_4-flow and CO_2-flow. As the CO_2 flow varies at a given SiH_4 and H_2 flow, the "true" hydrogen dilution with respect to the $[SiH_4 + CO_2]$ gas flow of course varies considerably. Possible effect on growth and material structure will have to be discussed. Further details of the gas flows and the used symbols in this work are summarized in Table I.

In the a-Si:H/μc-Si:H tandem solar cell we used an n-type microcrystalline silicon (μc-Si:H <n>) layer in the a-Si:H top cell, therefore in the tandem cell the μc-SiO_x:H intermediate reflector grows on a microcrystalline layer which might act as seed layer. This means the nucleation conditions are different compared to the conditions on the bare glass substrate. To obtain similar growth conditions for the μc-SiO_x:H films we use a very thin highly crystalline μc-Si:H <n> layer as seed layer for some films for comparison.

B. Solar cell preparation and properties

Figure 1 shows the a-Si:H/μc-Si:H solar cells configuration in which the influence of the SiO_x:H <n> intermediate reflector was investigated. The substrate for these cells was SnO_2:F coated glass. The cells are grown in pin/pin configuration. All layers were deposited using PECVD technology. For the a-Si:H top cell the <p> layer and the <i> layer are amorphous, the <n> layer is microcrystalline. The 70 nm thick SiO_x:H <n> intermediate reflector is grown between this top-cell <n> layer and the subsequent layer of the bottom cell. The bottom cell materials are all microcrystalline, using optimum phase mixture (OPM) material[19] for the μc-Si:H absorber layer. The deposition parameters of the intermediate reflector in the solar cell were varied as described in Sec. II A. A zinc oxide/silver (ZnO/Ag) layer stack on top of the μc-Si:H bottom cell was used as back contact.
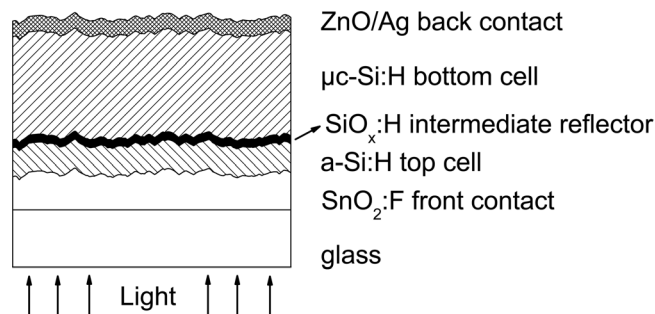

FIG. 1. A schematic drawing of the a-Si:H/μc-Si:H tandem solar cell with SiO_x:H intermediate reflector.

C. Characterization methods for films and solar cells

The optical, structural and electrical properties of the layers were investigated by optical transmission and reflection spectroscopy, photo thermal deflection spectroscopy (PDS), Raman spectroscopy ($\lambda = 488$ nm), Rutherford back scattering (RBS)[20,21] and dark conductivity measurements.

From conductivity measurements with coplanar Ag-electrodes, we obtain the lateral conductivity (σ) of the samples. To examine the crystalline volume fraction of the material, Raman spectroscopy was used. We define the Raman intensity ratio I_c as the ratio of the integrated area of the μc-Si:H peak at 520 cm^{-1} to the total peak area (a-SiO$_x$:H + μc-Si:H). The ratio is

$$I_C = \frac{A_{\mu\text{c-Si:H}}}{A_{\mu\text{c-Si:H}} + A_{\text{a-SiO}_x\text{:H}}} = \frac{A_{\mu\text{c-Si:H}}}{A_{\mu\text{c-SiO}_x\text{:H}}} \qquad (3)$$

where we define $A_{\mu\text{c-Si:H}} + A_{\text{a-SiO}_x\text{:H}} = A_{\mu\text{c-SiO}_x\text{:H}}$. The procedure is illustrated in Fig. 2 showing the corresponding peaks. To extract the peak areas we used the a-SiO$_x$:H reference peak which is measured on a sample grown in the amorphous regime with a high r_{CO_2} expected to be completely amorphous. When fitting the a-SiO$_x$:H reference peak to the measured μc-SiO$_x$:H peak one gets as difference a typical μc-Si:H peak. The integrated area of the total μc-SiO$_x$:H peak $A_{\mu\text{c-SiO}_x\text{:H}}$ and the integrated area of the μc-Si:H peak $A_{\mu\text{c-Si:H}}$ are used to calculate the I_c with Eq. (3). We should note the following problem for the evaluation of the crystallinity of the material from the Raman spectroscopy: (i) The absorption coefficient of a-SiO$_x$:H is about a factor ten lower compared to the absorption coefficient of μc-Si:H at the laser wavelength of 488 nm used for the Raman spectroscopy. Besides the unknown changes of Raman cross sections for the materials this will lead to an overestimation of the μc-Si:H phase when calculating the I_c for layers with higher oxygen contents. (ii) For μc-SiO$_x$:H films which are grown on a seed layer, in addition the Raman signal generated by the light reaching the μc-Si:H-seed layer might contribute to the calculated value of I_c. So care has to be taken when using these I_c values as a measure of crystallinity.

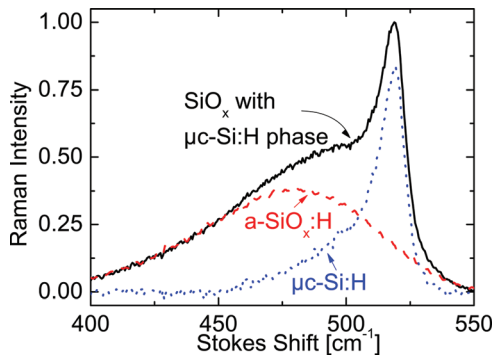The refractive index (n) versus the wavelength was determined using the layer thickness (d) measured by a step profiler and the maxima (λ_1) and minima (λ_2) of the interference fringes in the optical transmission and reflection spectra measured using a UV-VIS-NIR photo spectrometer. To calculate the refractive index we used the formula

$$n = \frac{1}{4d\left(\frac{1}{\lambda_1} - \frac{1}{\lambda_2}\right)} \qquad (4)$$

with which we determined the refractive index at a wavelength of 1 μm.

The IV-parameters for the tandem cells e.g., fill factor (FF), short circuit current density (j_{sc}) and open circuit voltage (V_{oc}) were measured using a double source (Class A) AM 1.5 sun simulator. To measure the current density of the component cells (j_{top}, j_{bot}) a quantum efficiency set-up was used. The reflected light of the complete solar cell from the glass side including the back reflector was measured using a UV-VIS-NIR photo spectrometer with attached Ulbricht sphere. The external quantum efficiency (QE) and the optical reflection spectra give insight in the optical gains and losses introduced by the intermediate reflector by comparing spectra of cells with and without intermediate reflector.

III. RESULTS

A. Material

1. Deposition rate

The deposition rate (r_D) of the SiO$_x$-layers was studied to be able to control the growth and intermediate reflector thickness in the cell. In Fig. 3, r_D is shown as a function of the CO$_2$/SiH$_4$-ratio (r_{CO_2}) for different hydrogen dilutions (ϕ_{SiH_4}: ϕ_{H_2}). For all series with a $\phi_{\text{SiH}_4} = 1$ sccm, r_D increases with decreasing hydrogen dilution by a factor of up to four. This is the most dominant trend and demonstrates the influence of the hydrogen dilution on the growth of the SiO$_x$. Another trend is the increase in deposition rate as a function of the r_{CO_2} for $r_{\text{CO}_2} > 0.5$. Increase of the silane flow at a given dilution (2:500) results in a strong increase in the deposition rate. Surprisingly for this series, we observe a decrease in the deposition rate as the CO$_2$ flow is increased.
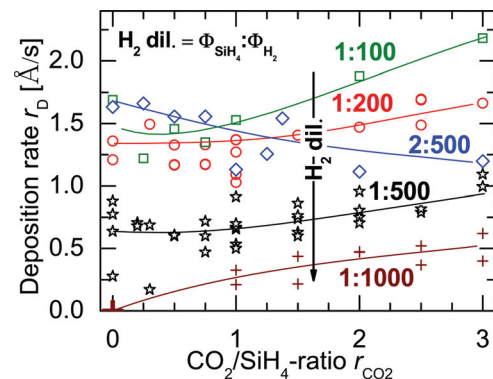

FIG. 2. (Color online) The normalized Raman intensity as a function of the stokes shift for a μc-SiO$_x$:H layer (compact line). The spectra of the μc-SiO$_x$:H layer is deconvoluted in an a-SiO$_x$:H peak (dashed line) and a μc-Si:H peak (dotted line) to calculate the crystalline volume fraction.

FIG. 3. (Color online) The deposition rate (r_D) vs the CO$_2$/SiH$_4$-ratio (r_{CO_2}). The SiH$_4$-flow and the H$_2$-flow used are indicated in sccm in the legend as H$_2$-dil. The lines are a guide to the eye.
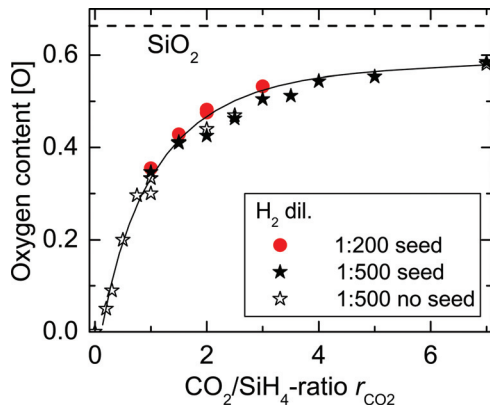
FIG. 4. (Color online) The oxygen concentration [O] as a function of the r_{CO_2}. The SiH_4-flow and the H_2-flow used are indicated in sccm in the legend as H_2-dil. The filled symbols stand for the samples with a seed layer and the open symbols represent the samples without seed layer. The [O] of SiO_2 is shown for comparison (dashed line). The line is a guide to the eye.

FIG. 5. (Color online) The Raman intensity ratio I_c as a function of the r_{CO_2} for layers with (filled symbols) and without seed layer (open symbols). The SiH_4-flow and the H_2-flow used are indicated in sccm in the legend as H_2-dil. The dashed lines are a guide to the eye for the films without seed layer. The compact lines are a guide to the eye for the films with see layer.

2. Oxygen concentration

Figure 4 shows the oxygen content [O] in the μc-SiO_x:H-films as determined by RBS depending on the r_{CO_2} for some of the series. [O] is defined as the ratio of oxygen in the alloy, i.e., [O] may vary from 0 to 0.66. A similar increase of incorporated oxygen with increasing r_{CO_2} is observed for the two H_2-dilution series with only a little lower [O] at higher hydrogen dilution. The oxygen content can be well controlled between 0 and 0.59. An oxygen content of 0.66 is the expected value for SiO_2 material. This value is shown as dotted line in the graph. The oxygen content [O] increases strongly for $0 < r_{CO_2} < 2$, for higher CO_2/SiH_4-ratios up to seven the [O] increases less steeply. Also note that the series with a H_2-flow of 500 sccm with and without seed layer result in very similar oxygen contents. Based on this result, we assume similar oxygen incorporation as a function of the CO_2/SiH_4 ratio also for other series prepared under similar conditions and use the data of Fig. 4 for calibration in case no RBS measurements for determination of the oxygen content were performed.

3. Crystallinity

The Raman intensity ratio (I_c) is shown versus the r_{CO_2} in Fig. 5 for films with and without seed layer and with different hydrogen dilutions (1:200, 1:500). For all series I_c decreases with increasing r_{CO_2}. However, the degree of decrease in crystallinity with CO_2 admixture depends on the preparation details, i.e., whether or not a seed layer is used. The use of a microcrystalline seed layer tends to enhance the I_c of the μc-SiO_x:H layers especially close to the transition to completely amorphous material. The increase in I_c is visible for both the 1:200 series between r_{CO_2} 0.5 to 1 and for the 1:500 series between r_{CO_2} of two and three even for layers of several hundreds of nanometers. Previous studies[22–26] have already shown the critical dependence of the film properties on the "substrate"-layer morphology especially in the transition region between a-Si:H and μc-Si:H growth. These studies show that layers deposited in the transition region grow completely amorphous or microcrystalline in dependence on the
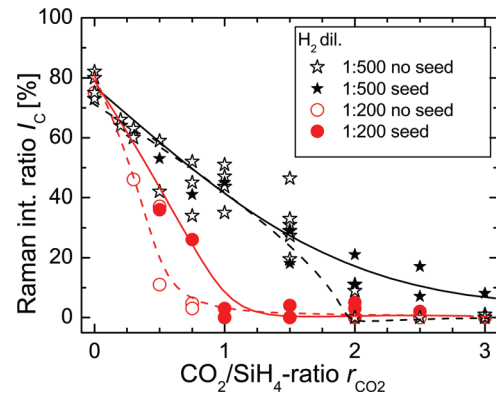
crystallinity of the "substrate" layer. For the intermediate reflector when it is applied as a thin layer in the solar cell the effect of the seed layer, which is the μc-Si:H n-layer of the top cell, might be even stronger. Focusing on the material without seed layer now, additional data on I_c for a wider range of hydrogen dilution is shown in Fig. 6(a), where we can directly compare the changes in crystallinity with the corresponding changes in conductivity [Fig. 6(b)]. Again, the crystallinity decreases for all series as the r_{CO_2} and therefore the oxygen content in the film increases. At a given r_{CO_2} an
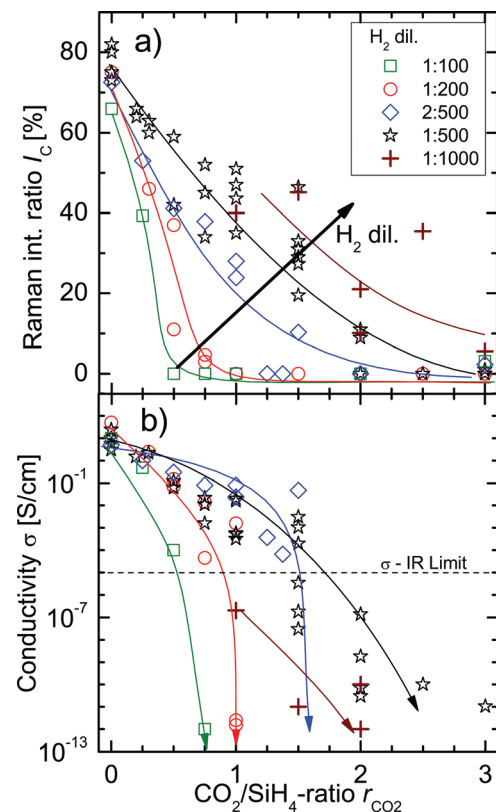

FIG. 6. (Color online) (a) The Raman intensity ratio I_c in dependence of the r_{CO_2}. (b) The conductivity σ vs the r_{CO_2}. The lower IR conductivity limit (σ-IR limit) is indicated (dashed line). The SiH_4-flow and the H_2-flow used are indicated in sccm in the legend as H_2-dil. The lines are a guide to the eye.

increase in H_2-dilution from 1:100 up to 1:1000 results in higher values of I_c in the transition between microcrystalline and amorphous growth. Pronounced scatter is observed for the values for I_c and σ for different layers deposited under the same conditions because of their critical dependence on the deposition parameters in the transition region. Especially little variations of gas flows will influence the growth and material properties. If one assumes a plausible variation of the CO_2 flow at 1 sccm of 10%, the expected change of the material properties in the transition region is large. However, the general trends discussed here are not affected by this data scatter. At the 1:500 hydrogen dilution used here, crystalline growth is still observed for $r_{CO_2} = 2$ which results in oxygen concentrations of 44% (Fig. 3). So oxygen-rich μc-SiO_x:H material with high optical transparency (see below), but still containing crystallinity phase of the order of 10% even without seed layer can be prepared at sufficiently high hydrogen dilution in the process gas.

4. Conductivity

Electrically the intermediate reflector represents an additional series resistor (R_s) between the two component cells which reduces the FF and therefore, the efficiency (η). To estimate the influence of the intermediate reflector on the FF we added numerically an Ohmic IV-characteristic of a series resistance R_s corresponding to the resistance of the intermediate reflector to a measured IV-characteristic of our standard tandem solar cell. For an additional series resistance of 1 Ω cm^2 we calculated a decrease in FF of about 1%. When increasing this series resistance to 10 Ω cm^2 we expect a drop in FF of about 7%. A similar dependency between R_s and FF was also found in.[27] Based on these calculations we set the highest acceptable additional series resistance to be 1 Ω cm^2. This additional series resistance would be reached when using an intermediate reflector with a thickness of 100 nm and a conductivity of 10^{-5} S/cm. We define this conductivity value (10^{-5} S/cm) as lower acceptable conductivity for the intermediate reflector layer [σ (IR)-limit]. This σ (IR)-limit is indicated by the dotted line in Fig. 6(b) and Fig. 12.

The electrical conductivity (σ) was measured for all films in planar direction by using co-planar silver contacts. In Fig. 6(b) the electrical conductivity σ of the films versus the r_{CO_2} is shown. The σ decreases with an increasing r_{CO_2}. For all hydrogen dilution series the conductivity decreases to less than 10^{-12} S/cm for higher r_{CO_2}. A conductivity of 10^{-12} S/cm at a film thickness of 1 μm is the detection limit of our conductivity measurement set-up therefore no conductivities are shown below this value. The lines to the eye are indicating measured conductivities values below the limit of the conductivity measurement set-up by an arrow. When increasing the hydrogen dilution from 1:100 up to 1:500 the drop of the conductivity shifts toward higher r_{CO_2}. Obviously this drop in σ coincides with the decrease of the Raman intensity ratio [Fig. 6(a)]. A higher value of I_c results in higher conductivities. At the highest hydrogen dilution to 1:1000, in spite of high values of I_c, the conductivities are lower again at high r_{CO_2} values. This is in accordance with frequently observed results, that a too high hydrogen dilution in the pro-
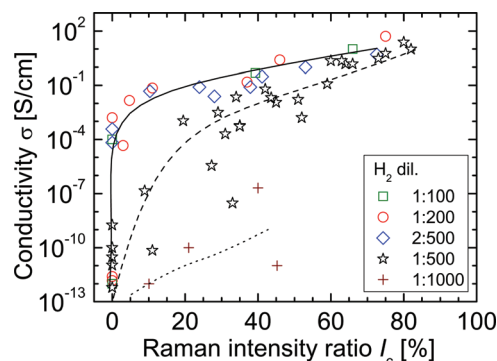

FIG. 7. (Color online) The conductivity vs the Raman intensity ratio for different hydrogen dilution series as indicated in the legend. The influence of the hydrogen dilution on the σ/I_c-dependence can be seen by the lines as guide to the eye for the different hydrogen dilutions. The dotted line is the guide to the eye for the 1:1000 hydrogen dilution series. The dashed line is the guide to the eye for the 1:500 hydrogen dilution series and the compact line for the other hydrogen dilution series.

cess gas might deteriorate the electrical properties of the material, possibly as a result of a too high etching contribution during the growth and therefore poor defect and grain boundary passivation in the material.[28]

To investigate the relationship between the conductivity and the crystalline volume fraction further, σ is also plotted in dependence of I_c in Fig. 7 for the different hydrogen dilution series. With increasing Raman intensity ratio the conductivity increases as expected when introducing a highly conductive μc-Si:H n-type phase. For films with a very low I_c the electrical conductivity is most likely dominated by the low σ of the amorphous SiO_x phase, where the doping efficiency is much lower due to the strong compensation by deep defects. For hydrogen dilution series 1:100, 1:200 and 2:500 the conductivity increases to values above 1×10^{-3} S/cm already at low Raman intensity ratios ($\sim$5%). At higher hydrogen dilution of 1:500 a Raman intensity ratio of 35% is needed to achieve a conductivity of 1×10^{-3} S/cm. For these series the decrease in σ coincides with the decrease of the Raman intensity ratio. For the 1:1000 hydrogen dilution series conductivities are well below all other hydrogen dilution series in spite of high values of I_c. As already described above, we attribute this to the too bad material quality, which results in low doping efficiency or a disruption of the current path. We conclude that, even for low I_c, highly conducting SiO_x films can be obtained by employing an appropriate hydrogen dilution.

For samples with seed layer, the planar conductivity was dominated by the highly conductive μc-Si:H <n> seed layer which acts as a short cut for the charge transport. Here the conductivity of the μc-SiO_x:H bulk material can not be determined.

5. Optical bandgap and refractive index

As optical bandgap (E_{04}), we use the photon energy value for which an optical absorption coefficient of 1×10^4 cm^{-1} is reached. The E_{04} values are shown as a function of the r_{CO_2} for different hydrogen dilution series in Fig. 8. The bandgap increases with increasing r_{CO_2}. It covers a range from below 2 eV up to a value of 2.9 eV. Increasing the silane flow at a given dilution (500), results in lower optical gaps for each CO_2 flow.
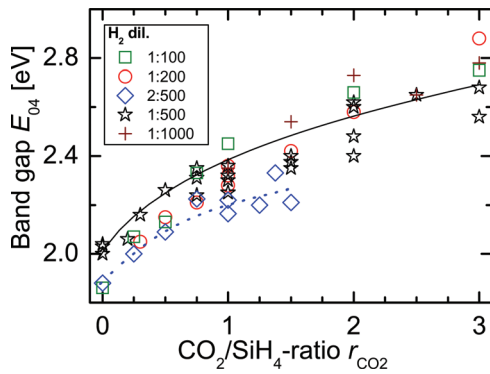
FIG. 8. (Color online) The bandgap vs the r_{CO_2} for films deposited using different hydrogen dilutions. The SiH_4-flow and the H_2-flow used are indicated in sccm in the legend as H_2-dil. The dotted line is a guide to the eye for the 2:500 hydrogen dilution series and the solid line for the other hydrogen dilution series.

FIG. 10. (Color online) The E_{04} as a function of the r_{CO_2} for layers with (filled symbols) and without seed layer (open symbols). The SiH_4-flow and the H_2-flow used are indicated in sccm in the legend as H_2-dil. The E_{04} as function of the oxygen content for amorphous silicon oxide films (a-SiO$_x$:H<n>) from literature (Ref. 30) are shown for comparison.

To study the link between the optical properties and the structural properties of the films the E_{04} is displayed versus the I_c for different hydrogen dilutions in Fig. 9. With increasing Raman intensity ratio the bandgap decreases for all hydrogen dilution series, starting at values up to 2.95 eV for low I_c. For high I_c we find $E_{04} = 1.9$ eV, which is a typical value for μc-Si:H n-type material. Two effects result in this decrease in E_{04} with increasing I_c: (i) the SiO$_x$:H-phase is replaced by the lower band-gap μc-Si:H phase and (ii) the bandgap in the a-SiO$_x$:H-phase decreases because of lower oxygen content. The initial drop in the bandgap versus crystallinity for the lower hydrogen dilutions (1:100–2:500) is steeper in accordance with the sharp drop in crystallinity with r_{CO_2} at low H dilution. At a given Raman intensity ratio I_c, e.g., 40%, the bandgap increases with increasing hydrogen dilution. Again, this can be explained by the higher oxygen content in the remaining amorphous SiO$_x$ fraction for a given I_c. This higher oxygen content is caused by the higher r_{CO_2} when depositing under the higher hydrogen dilution conditions or in other words, at higher hydrogen dilution the material still develops a microcrystalline phase at considerably higher CO$_2$ flows.

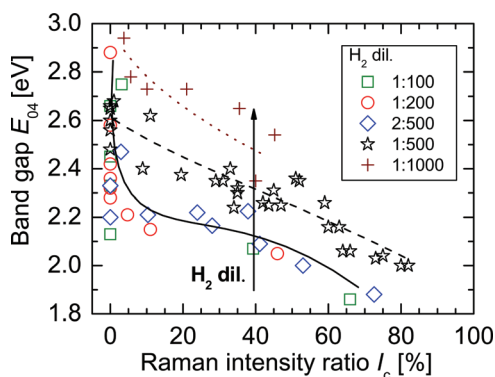To relate the bandgap to the film composition, Fig. 10 shows the bandgap versus the incorporated oxygen [O] for the

1:200 and 1:500 hydrogen dilution series for layers with and without seed layer. There is little difference in the values of E_{04} at a given [O] for both hydrogen dilutions (1:200, 1:500) and between layers with and without seed layer. The E_{04} is increasing from 1.9 eV to 2.5 eV when reaching a [O] of 0.5. For oxygen contents larger than 0.5 the increase of the E_{04} becomes more pronounced with increasing r_{CO_2} and reaches 2.8 eV for [O] of 0.6. This more pronounced increase in E_{04} can be understood by considering the strong bandgap increase for oxygen contents >0.5 to 8.9 eV of SiO$_2$ (Ref. 29). For comparison we also show the dependence of the optical bandgap versus [O] for a-SiO$_x$:H (Ref. 30). At low [O] this material shows a lower E_{04} than our μc-SiO$_x$:H. At high oxygen content the remaining μc-phase on the other hand leads to lower E_{04} in the μc-SiO$_x$:H material.

The material's refractive index is a most crucial parameter for application of the material as intermediate reflector. The refractive index is calculated as described in Sec. II C. It is plotted versus r_{CO_2} in Fig. 11. When increasing the r_{CO_2} from zero to three the refractive index decreases from 3.8 for μc-Si:H down to values close to 1.5, i.e., the value of pure SiO$_2$. Again we find a little different behavior between

FIG. 9. (Color online) The E_{04} vs the I_c. The SiH_4-flow and the H_2-flow used are indicated in sccm in the legend as H_2-dil. The dotted line is the guide to the eye for the 1:1000 hydrogen dilution series. The dashed line is the guide to the eye for the 1:500 hydrogen dilution series and the compact line for the other hydrogen dilution series.
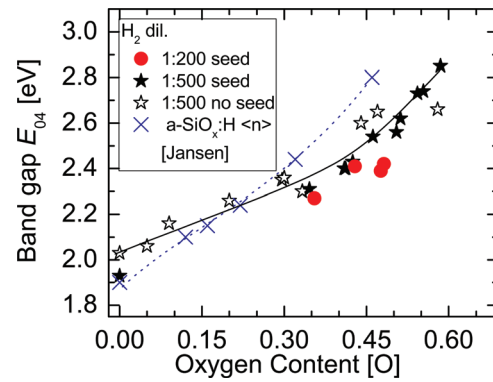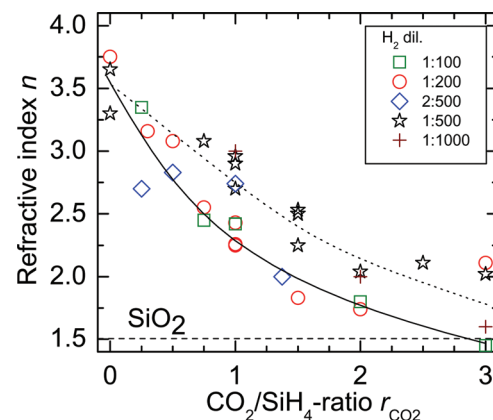

FIG. 11. (Color online) The refractive index n vs the r_{CO_2} for films using different hydrogen dilutions. The $n(SiO_2)$ is shown for comparison (dashed line). The SiH_4-flow and the H_2-flow used are indicated in sccm in the legend as H_2-dil. The dotted line is the guide to the eye for the 1:500 hydrogen dilution series and the compact line for the other hydrogen dilution series.

materials prepared at low (1:100–2:500) and high (1:500 and 1:1000) hydrogen dilution respectively. At higher H_2 dilution we find higher refractive indices for a given r_{CO_2}. Still a similar trend of decreasing n with increasing r_{CO_2} is observed. We can summarize that the material's refractive index n can be easily varied and controlled using appropriate gas mixtures for the μc-SiO$_x$:H preparation.

6. Electrical conductivity versus optical bandgap and refractive index

The relationship between optical and electrical properties is the central point in the development of the μc-SiO$_x$:H $<n>$ as a functional layer. A low refractive index and a high bandgap at a sufficient conductivity are desired for the use as intermediate reflector. We suggest that a plot of conductivity versus refractive index and optical bandgap, like in Fig. 12 can serve as a figure of merit for the suitability of the silicon oxide as an intermediate reflector layer. High conductivities were found for high refractive indices and low band gaps. However, for lower refractive indices and high band gaps, as desired for the use as intermediate reflector, the conductivity is reduced. When a conductivity similar to a-Si:H $<n>$ ($\sigma \approx 10^{-3}$ S/cm) is reached, σ drops sharply for a further decrease of n and increase of E_{04}. The aforementioned defined σ(IR)-limit is plotted as dotted line in the graph. Also shown are corresponding dark conductivities for a-SiO$_x$:H.[25] All samples prepared by different series fall, within certain scatter, on the similar trend lines σ versus E_{04} and n respectively. Therefore, the relationships between electric and optical properties in the material prepared here are more determined by the material structure and composition rather than by the differences in the deposition processes. We find material with a wide range of optical properties, large bandgap and low refractive index as compared to a-Si:H and μc-Si:H, and for the series using a hydrogen dilution 1:200, 2:500 and 1:500 with conductivities well above the σ(IR)-limit. Within the 1:100 hydrogen dilution series lower conductivities for a
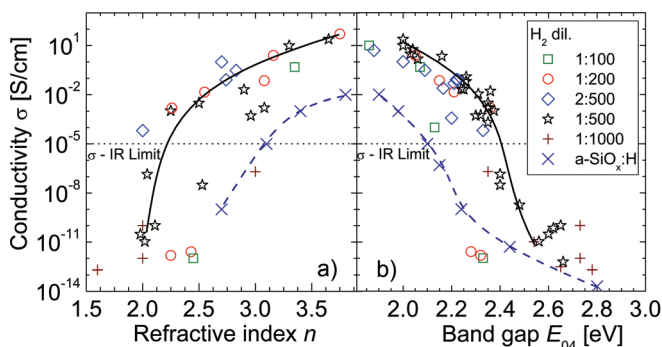
given band gap were obtained. For the 1:1000 hydrogen dilution series the conductivity is below the calculated limit suitable for the use as IR in solar cells.

The low refractive index may provide a distinct refractive index step compared to $n_{a-Si:H} \approx 3.7$ at sufficient electrical conductivity. This means the material has considerable potential to serve as IR with excellent compromise between conductivity and refractive index. For comparison a-SiO$_x$:H $<n>$ without a μc-Si:H phase shows electrical conductivity up to seven orders of magnitude smaller than that of the μc-SiO$_x$:H $<n>$ films. At the σ(IR)-limit the a-SiO$_x$:H $<n>$ has a too high n of 3.1 and a low E_{04} of 2.05 eV. Thus only the introduction of a microcrystalline phase in the alloy enables a proper combination of electrical and optical properties for the use as intermediate reflector.

These results are for films without seed layer only. The influence of the seed layer on the electrical conductivity of the intermediate reflector material can not be evaluated by simple conductivity measurements. But to some extent the beneficial influence of the seed layer on electrical conductivity becomes obvious when the material is used as intermediate reflector in the tandem solar cells, where growth conditions for the IR, which on glass would result in very low conductivity, in the cell still, result in highly efficient performance and high FF.

B. Solar cells

The gains and losses when applying the μc-SiO$_x$:H layers as intermediate reflector (IR) were evaluated in a-Si:H/μc-Si:H tandem solar cells. The influence of the IR on the optical performance of tandem cells was investigated by external quantum efficiency (QE) and optical reflection. The influence on the electrical properties of the solar cell was mainly concluded from the cell's FF. Figure 13 shows the FF of the best 1 cm^2 tandem cell on each 10 × 10 cm^2 substrate for different deposition conditions of the IR. The deposition conditions for the IR are the same as for the corresponding layers discussed in Sec. III A. A FF of 72% which is similar to cells without IR serves as a benchmark and is

FIG. 12. (Color online) The electrical conductivity σ for μc-SiO$_x$:H films without seed layer with different hydrogen dilutions as given in the caption as a function of the refractive index n (a) and the bandgap E_{04} (b), respectively. The SiH$_4$-flow and the H$_2$-flow used are indicated in sccm in the legend as H$_2$-dil. The characteristics of amorphous silicon oxide films (a-SiO$_x$:H$<n>$) from literature (Ref. 30) are shown for comparison. In both graphs the calculated lower conductivity limit σ(IR)-limit for the use as intermediate reflector is indicated as dotted line. The dashed line is a guide to the eye for the literature values and the solid line is a guide to the eye for the other films.
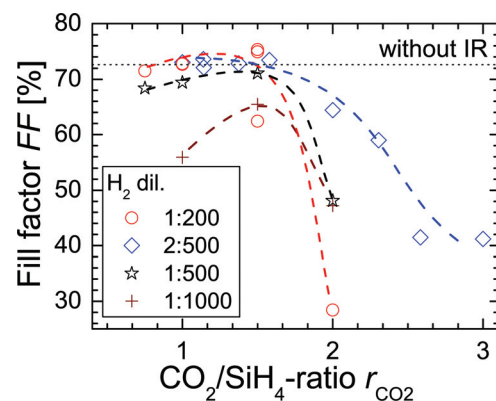

FIG. 13. (Color online) The fill factor of the tandem solar cells vs the r_{CO_2} for the different hydrogen dilutions applied during intermediate reflector deposition. The SiH$_4$-flow and the H$_2$-flow used are indicated in sccm in the legend as H$_2$-dil. The dotted line represents the fill factor of a tandem solar cell without intermediate reflector. The lines are a guide to the eye.

indicated by a dotted line. For $r_{CO_2} \leq 1.5$ and hydrogen dilution up to 1:500 the *FF* remains at a high value. For higher r_{CO_2} it decreases considerably. At a hydrogen dilution of 1:1000 the *FF* is well below the benchmark for all r_{CO_2}.

Note that SiO_x material prepared at 1:200 and 2:500 and r_{CO_2} of 1.5 and 2, respectively, when deposited on glass substrate, has a planar conductivity below 10^{-12} S/cm [Fig. 6(b)]. This should result in a strong increase of the cells series resistance and thus in a low *FF*. The yet successful implementation without large decrease in *FF* might be attributed to the increased crystalline volume fraction introduced by the μc-Si:H $<n>$ layer which acts as seed layer for the growth of the μc-SiO_x:H IR. Another possibility is a higher conductivity in vertical than in planar direction.[12]

In Table II, the results of the IV- and QE-measurements for an a-Si:H/μc-Si:H tandem solar cell of 1 cm² with a μc-SiO_x:H $<n>$ intermediate reflector film deposited using a hydrogen dilution of 1:500 and a r_{CO_2} of 1.5 with a refractive index of 2.25 and $E_{04} = 2.35$ eV are shown. An increase in top cell current density of 1.3 mA/cm² with similar *FF* and V_{oc} compared to cells without an intermediate reflector is achieved. An efficiency of 11.5% is reached at a top cell absorber layer thickness of only 250 nm. To see the effect of the SiO_x IR in detail, the quantum efficiency of the above-mentioned tandem cell with and without SiO_x IR is shown in Fig. 14(a) (compact and dashed graph, respectively). The enhanced QE for the top cell in the wavelength region between 500 nm and 800 nm with a μc-SiO_x:H IR is obvious. The incident light is reflected back at the interface between top cell and intermediate reflector and therefore transferred from the bottom cell to the top cell. The top cell current density increases by 1.3 mA/cm² and the bottom cell current density decreases by 1.3 mA/cm². The current matching requirements are almost fulfilled with a top cell current density of 11.3 mA/cm² and bottom cell current density of 11.4 mA/cm² for this tandem solar cell by introducing the μc-SiO_x:H intermediate reflector while keeping the sum of both cell currents constant. The high bandgap of 2.3 eV appears to be big enough to avoid losses due to parasitic light absorption.

Possible losses due to increased reflection of light out of the cell when applying an intermediate reflector were investigated by optical reflection measurements on the cell using a photo spectrometer with attached Ulbricht sphere. The optical reflection is shown in dependence of the wavelength in Fig. 14(b) for the cell with and without IR (compact and dashed graph, respectively). Between 650 nm and 800 nm the reflection is slightly higher for the cell with IR. However, these losses are compensated for by the total gain in QE between 500 nm and 650 nm as apparent from Fig. 14(a).

The influence of the SiO_x intermediate reflector on the current density of the a-Si:H top cell and the μc-Si:H bottom
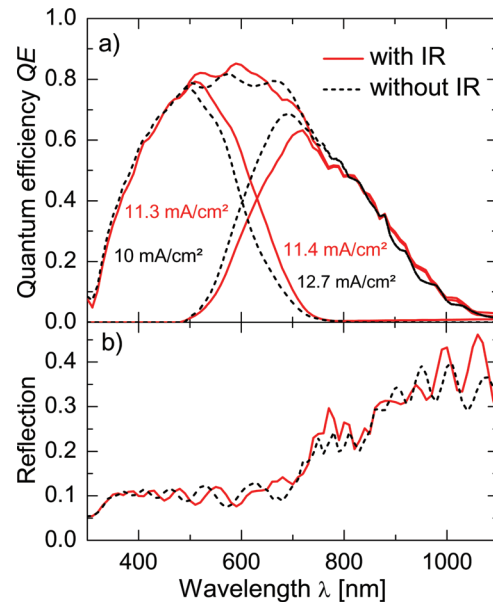

FIG. 14. (Color online) (a) The quantum efficiency *QE* and (b) the reflection for a cell with intermediate reflector are shown as a compact line and for a cell without intermediate reflector as a dotted line.

cell was evaluated from quantum efficiency measurements. In Figs. 15(a) and 15(b), the current density of the component cells are plotted versus r_{CO_2} for different hydrogen dilution series. The results of the best 1 cm² solar cell of each 10×10 cm² substrate are shown. Therefore, the scatter of the results for specific deposition parameters has its origin in different solar cell deposition runs. Intermediate reflectors using a hydrogen dilution of 1:100 were not implemented due to their poor optical properties above the conductivity limit.

In general, the top cell current increases with increasing r_{CO_2} for all applied intermediate reflectors prepared under a variety of preparation conditions. The highest top cell current density obtained was 12.5 mA/cm² for a cell with $r_{CO_2} = 2.5$ and a hydrogen dilution of 2:500. Similarly the current density for the μc-Si:H bottom cell decreases with increasing r_{CO_2} by about the same amount [Fig. 15(b)]. Consequently we observe, especially for the IR prepared with hydrogen dilution of 1:200 and 2:500, a constant sum of both current densities (top + bottom) over a wide range of r_{CO_2} [Fig. 15(c)] with values close to 23 mA/cm² which was found for the tandem solar cell without intermediate reflector. The SiO_x intermediate reflector works without additional optical losses over a wide range of deposition conditions.

For the cells presented so far we kept the thickness of the component cells constant and varied the r_{CO_2} and hydrogen dilution for the intermediate reflector. In the following studies, a certain intermediate reflector deposited using a hydrogen dilution of 1:500 and a r_{CO_2} of 1.5 was implemented in tandem solar cells for which we varied the thickness of the top cell while keeping the bottom cell's thickness constant at 1.8 μm. For comparison, the same was done for tandem cells without intermediate reflector. The resulting currents for top and bottom cell calculated from QE measurements are shown as a function of the top cell thickness in Fig. 16. For both cell configurations the top solar cell's current density increases with the top cell's thickness, while the current density of the
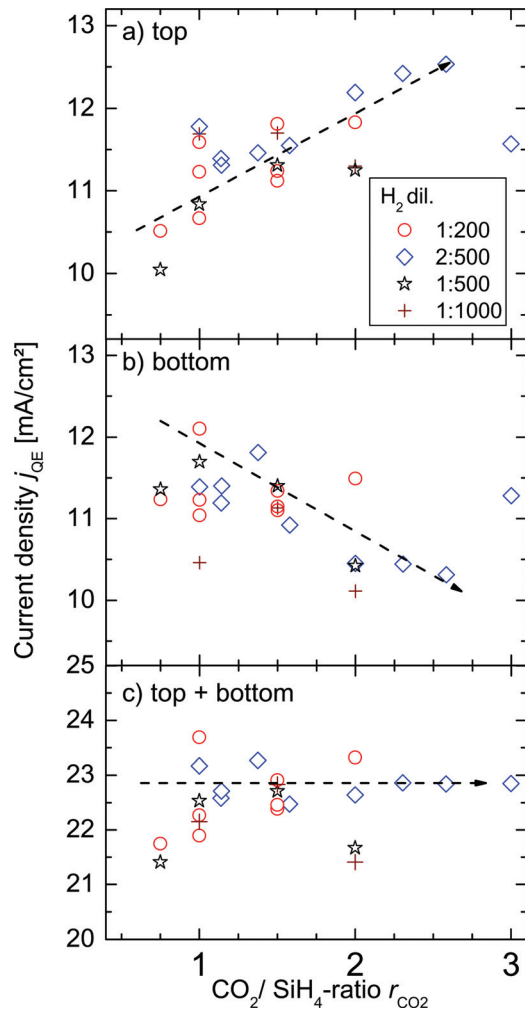
TABLE II. The solar cell parameters of the a-Si:H/μc-Si:H tandem solar cells with and without intermediate reflector.

	η %	V_{oc} V	*FF* %	j_{top} mA/cm²	j_{bot} mA/cm²
No IR	10.0	1.36	73	10.0	12.7
IR	11.5	1.37	74	11.3	11.4

FIG. 15. (Color online) The current density for the component solar cells calculated from the quantum efficiencies vs the r_{CO_2} for different hydrogen dilutions. The SiH$_4$-flow and the H$_2$-flow used are indicated in sccm in the legend as H$_2$-dil. The current density for the a-Si:H top solar cell, for the μc-Si:H bottom cell and sum of the individual cells are shown in (a), (b) and (c), respectively. The lines are a guide to the eye.
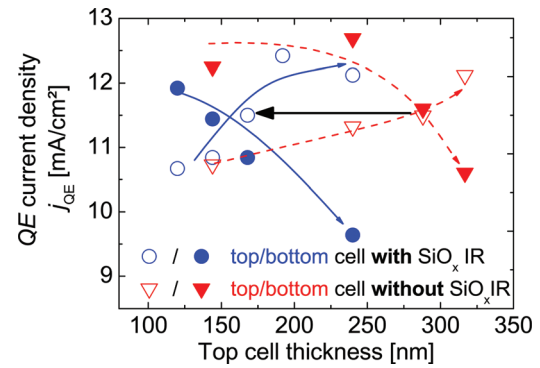

FIG. 16. (Color online) The short circuit current densities calculated from the quantum efficiency for top cells (filled symbols) and bottom cells (open symbols). The circles indicate the cells with intermediate reflector, the triangles the cells without intermediate reflector. The dashed lines are a guide to the eye for the cells without IR and the solid lines are for the cells with IR.

With this one can think of decoupling the electronic and optical functionality of the material into its two phases. In addition the preparation process with PECVD at about 200 °C, with standard source gases and also otherwise typical deposition conditions similar to thin film silicon processes makes it straightforward to implement the IR into cells prepared with similar conditions in the same deposition system.

Starting from highly conductive μc-Si:H(P) the addition of [O], in order to get low refractive index material, results in break-down of crystalline growth already at low [O] resp. CO$_2$ flow concentration. The electrical conductivity depends strongly on the crystalline volume fraction. In order to still obtain sufficient conductivity, the crystal growth break-down can be counteracted by appropriate hydrogen dilutions. However, at the highest hydrogen dilutions the conductivity is reduced despite of a high crystalline volume fraction which might be attributed to a defect-rich μc-Si:H <n> phase in this case as a result of too strong etching contribution during the growth process. On the other hand at lower hydrogen dilution high conductivities even for low Raman intensity ratios are observed suggesting a high quality and highly conductive current path through the doped μc-Si:H phase.

In addition, it can be concluded that the current transport is promoted in direction of growth i.e., in direction of current flow inside the tandem cell. This is attributed to the columnar structure of the crystalline regions in the μc-SiO$_x$:H compound. This columnar structure is possibly further enhanced by the nucleation of the μc-SiO$_x$:H layer on the highly crystalline μc-Si:H(P) layer of the top cell. Connected with this is the finding that material which results in high efficiently solar cells with high fill factor, would on glass give very low conductivities.

This critical substrate dependence of the nucleation and growth—seen as an advantage here as one can grow with higher [O] content and still get high conductivity—is a challenge for reliable material studies, e.g., for investigating the conductivities parallel and perpendicular to the growth axis. It will be also a challenge, in case one wants to replace the top cell n-layer, in this case the μc-SiO$_x$:H would have to serve also as a field-build-up layer of the top cell. The influence of [O] content or CO$_2$ admixture on the material growth with break-down of the crystal growth would have to be investigated in more detail considering the effect of hydrogen

bottom cell decreases. For tandem solar cells without IR a top cell thickness of 290 nm is needed to reach a current matching between the individual cell currents. For a tandem solar cell with intermediate reflector, however, a top cell thickness of only 150 nm is sufficient to meet the current matching requirement. This demonstrates the potential to achieve current matching at a similarly high current with a much thinner top cell by using an n-type μc-SiO$_x$:H intermediate reflector.

IV. DISCUSSION

As described in the Introduction, the intermediate reflector between the top and bottom cell of a thin film silicon based solar cell has to fulfill a number of requirements on its electrical and optical properties. This makes it generally difficult to find and optimize a single material for this purpose but the phosphorus doped μc-SiO$_x$:H material investigated here proofs to be very suitable. The material is a composite of highly conductive μc-Si:H(P) phase and an a-SiO$_x$:H phase where the optical transparency is closely linked to the [O] content and the conductivity is low because of the known poor doping efficiency.

dilution. This means, like for other Si-alloys, one should consider in how far the ratio of $[SiH_4 + CO_2]$ versus $[H_2]$ as a parameter is mainly responsible for the microcrystalline-to-amorphous transition. This will be preserved for future studies.

Tuning the trade-off between a highly conductive μc-Si:H fraction and an a-SiO$_x$:H phase with high oxygen content yields a material with a combination of low refractive index and high bandgap at sufficient conductivity ($E_{04} = 2.4$ eV, $n = 2.1$ at $\sigma = 10^{-5}$ S/cm). Judging from the material properties, the series with hydrogen dilutions of 1:200, 2:500, and 1:500 look most promising for the use as an IR. This is supported by the solar cell results. The 1:1000 hydrogen dilution is not found suitable for growth of IR layers. Low conductivity and therefore fill factor losses in the solar cells are found for such material. For all series implemented in the tandem solar cell, the lower refractive index of SiO$_x$ compared to a-/μc-Si:H causes a current transfer from bottom to top cell.

We summarize: An intermediate reflector for thin film silicon solar cells was successfully developed on basis of a the compound material μc-SiO$_x$:H(P). The implementation of this IR allows to reduce the top cell thickness considerably while keeping the total cell current constant on a high level. This should finally result in considerably enhanced stability of the tandem cells against light induced degradation.

V. CONCLUSION

μc-SiO$_x$:H is developed as an intermediate reflector in thin film silicon based tandem solar cells. The preparation of the phosphorus doped μc-SiO$_x$:H from SiH$_4$, CO$_2$, PH$_3$, and H$_2$ source gases results in a phase mixture material of highly conductive microcrystalline μc-Si:H(P) and an amorphous a-SiO$_x$:H in which the increase of the oxygen content [O] leads to high bandgap and low refractive index.

What could be considered a disadvantage in this material development, namely the distinct phase separation, turns out as an advantage for the application of the material as intermediate reflector. One can regard the electronic and optical functionality of the material as decoupled into the materials two phases.

The specific film properties for the use as intermediate reflector of the μc-SiO$_x$:H can be well controlled via the deposition conditions like CO$_2$ gas flow and hydrogen dilution. Implementing the μc-SiO$_x$:H intermediate reflector into tandem solar cells, a reduction of the top cell thickness of about 40% while maintaining the current matching requirements is demonstrated.

ACKNOWLEDGMENTS

[1]B. Rech and H. Wagner, Appl. Phys. A **69**, 155 (1999).

[2]S. Schicho, D. Hrunski, R. van Aubel, and A. Gordijn, Prog. Photovoltaics **18**, 83, (2010).

[3]J. Krc, S. Franc, and M. Topic, Sol. Energy Mater. Sol. Cells **86**, 537 (2005).

[4]P. Obermeyer, C. Haase, and H. Stiebig, Appl. Phys. Lett. **92**, 92 (2008).

[5]C. Rockstuhl, F. Lederer, K. Bittkau, T. Beckers, and R. Carius, Appl. Phys. Lett. **94**, 21110 (2009).

[6]D. Fischer, S. Dubai, N. Pellaton, A. J. A. Selvan, R. Platz, C. Hof, U. Kroll, J. Meier, P. Torres, H. Keppner, N. Wyrsch, M. Go, A. Shah, and K. D. Ufert, in *Proceedings of the 25th IEEE Photovoltaic Specialists Conference*, Washington DC, USA, IEEE Cat. No. 96CH35897 (IEEE, New York, 1996), pp. 1053–1056.

[7]J. Meier, J. Spitznagel, S. Fay, C. Bucher, U. Graf, U. Kroll, S. Dubail, and A. Shah, in *Proceedings of the 29th IEEE Photovoltaic Specialists Conference*, New Orleans, USA, IEEE Cat. No. 02CH37361 (IEEE, New York, 2002), pp. 1118–1121.

[8]J. Springer, Ph.D. dissertation, Institute of Physics, Academy of Sciences of the Czech Republic, 2004.

[9]L.V. Mercaldo, I. Usatii, P. Ciani, and C. Privato, in *Proceedings of the 24th European Photovoltaic Solar Energy*, Hamburg, Germany (WIP Renewable Energies, Munich, 2009), pp. 2723–2726.

[10]A. Sarker, C. Banerjee, and A. K. Barua, J. Phys. **35**, 1205 (2002).

[11]K. Yamamoto, A. Nakajima, M. Yoshimi, T. Sawada, S. Fukuda, and T. Suezaki, in *Record of the IEEE 4th World Conference on Photovoltaic Energy Conversion*, Waikoloa, USA, IEEE Cat. No. 06CH37747C (IEEE, New York, 2006), pp. 1489–1492.

[12]P. Buehlmann, J. Bailat, D. Dominé, A. Billet, F. Meillaud, A. Feltrin, and C. Ballif, Appl. Phys. Lett. **91** 143505 (2007).

[13]A. Lambertz, A. Dasgupta, W. Reetz, A. Gordijn, R. Carius, and F. Finger, in *Proceedings of the 22nd European Photovoltaic Solar Energy Conference*, Milan, Italy (WIP Renewable Energies, Munich, 2007), pp. 1839–1842.

[14]A. Lambertz, T. Grundler, and F. Finger, in *Proceedings of the 24th European Photovoltaic Solar Energy Conference*, Hamburg, Germany (WIP Renewable Energies, Munich, 2009), pp. 2402–2407.

[15]T. Grundler, A. Lambertz, and F. Finger, Phys. Status Solidi C **7**, 1085 (2010).

[16]C. Das, A. Lambertz, J. Huepkes, W. Reetz, and F. Finger, Appl. Phys. Lett. **92**, 053509 (2008).

[17]D. Dominé, P. Buehlmann, J. Bailat, A. Billet, A. Feltrin, and B. Christophe, Phys. Status Solidi (RRL) **2**, 163 (2008).

[18]V. Smirnov, W. Böttler, A. Lambertz, H. Wang, and R. Carius, Phys. Status Solidi C **7**, 1053 (2010).

[19]Y. Mai, S. Klein, R. Carius, J. Wolff, A. Lambertz, F. Finger, and X. Geng, J.Appl. Phys. **97**, 114913 (2005).

[20]B. Holländer, H. Heer, M. Wagener, H. Halling, and S. Mantl, Nucl. Instrum. Methods Phys. Res. B **161**, 227 (2000).

[21]W. K. Chu, J. W. Mayer, M. A. Nicolet, *Backscattering Spectroscopy* (Academic, New York, 1986).

[22]A. Lambertz, F. Finger, and R. Carius, in *Proceedings of 3rd World Conference on Photovoltaic Energy Conversion*, Volume B, edited by: K. Kurokawa, L. Kazmerski, B. McNelis, M. Yamaguchi, C. Wronski, and W. Sinke, Osaka, Japan, IEEE Cat. No. 03CH37497 (WCPEC-3 Organizing Committee, Osaka, 2003), pp. 1804–1807.

[23]V. Smirnov, C. Das, T. Melle, A. Lambertz, M. Hülsbeck, R. Carius, and F. Finger, Mater. Sci. Eng. B **159**, 44 (2009).

[24]O. Vetterl, M. Huelsbeck, J. Wolff, R. Carius, and F. Finger, Thin Solid Films **427**, 46 (2003).

[25]P. Roca, I. Cabarrocas, N. Layadi, T. Heitz, B. Drévillon, and I. Solomon, Appl. Phys. Lett. **66**, 3609 (1995).

[26]T. Fujibayashi and M. Kondo, J. Appl. Phys. **99**, 043703 (2006).

[27]B. Rech, Solarzellen aus amorphem Silizium mit hohem stabilem Wirkungsgrad, in Berichte des Forschungszentrums Jülich Vol. 3427, Jülich, 1997 .

[28]F. Finger, "Basic properties of hydrogenated microcrystalline silicon," in *Thin-Film Silicon Solar Cells*, edited by A. Shah, 1st ed. (EPFL Press, Lausanne, Switzerland, 2010).

[29]R. Carius, R. Fischer, E. Holzenkämpfer, and J. Stuke, J. Appl. Phys. **52**. 4241 (1981).

[30]R. Janssen, A. Janotta, D. Dimova-Malinovska, and M. Stutzmann, Phys. Rev. B **60**, 561 (1999).